Journal of Materials Chemistry A

RSC Publishing

PAPER

View Article Online
View Journal | View Issue

Cite this: J. Mater. Chem. A, 2013, 1, 7673

Chemical expansion and its dependence on the host cation radius

Dario Marrocchelli,*[abc] Sean R. Bishop[ad] and John Kilner[de]

Received 11th March 2013
Accepted 14th May 2013

DOI: 10.1039/c3ta11020f

www.rsc.org/MaterialsA

The defect-induced lattice expansion (chemical expansion), and corresponding relaxation patterns around oxygen vacancies, were examined as a function of host cation radius for HfO_2, ZrO_2, CeO_2, UO_2, ThO_2, and Bi_2O_3 fluorite-structured oxides. Analysis of data from the literature, combined with new molecular dynamics simulations, found a maximum in the effective radius of an oxygen vacancy (related to the lattice contraction around a vacancy) for a host cation size close to that of cerium. In other words, ceria shows the highest chemical expansion, whereas the other studied materials, with either smaller or bigger host cations than Ce, undergo smaller chemical expansion. Significant asymmetric lattice relaxation around a vacancy for smaller cations and 2nd nearest neighbor cation relaxations around a vacancy for larger cations play a strong role in forming the maximum. The impact of this vacancy relaxation on ionic conductivity is discussed, and through careful analysis of the vacancy–anion radial distribution functions, an estimate of a critical vacancy concentration ($c^* = 0.025\%$), above which vacancy interactions exist, was derived.

Introduction

Fluorite structured oxides are used in many high temperature energy applications such as electrodes and electrolytes for solid oxide fuel cells (SOFCs)[1,2] and oxygen permeation membranes, as well as oxygen storage materials for gas conversion/reformation catalysis[3–6] and thermochemical water splitting.[7] The above applications typically rely on rapid oxygen exchange with the atmosphere and diffusion in the material. For electrodes and oxygen storage materials, the kinetics for exchange of oxygen with the atmosphere in the former, and oxygen storage capacity in the latter, is enhanced by using materials displaying large oxygen deficiencies (non-stoichiometry), facilitated by the presence of a redox couple, such as $Ce^{4+/3+}$, resulting in mixed ionic and electronic conductivity.[1,7] Conversely, in electrolyte applications where only ionic conductivity is desired, acceptor dopants with fixed valence (*e.g.* Gd^{3+} in CeO_2 or Y^{3+} in ZrO_2), charge compensated by the formation of oxygen vacancies, are added. These cation and anion point defects result in significant changes in lattice dimension, known as *chemical expansion*. Indeed, many high performance SOFC electrodes and electrolytes exhibit significant oxygen stoichiometry fluctuations with changes in atmosphere (oxidizing to reducing) and temperature, thus resulting, *inter alia*, in significant mechanical stresses, followed by mechanical failure, from chemical expansion.[8] Additionally, local strain (in combination with electrostatic) effects near defects play a significant role in decreasing ionic mobility, having thus led to the formulation of a critical acceptor dopant radius in ZrO_2 and CeO_2 SOFC electrolytes.[9] Other examples of this phenomenon are the dramatic electrode expansion in Li-ion batteries during Li intercalation (sometimes termed electrochemical shock[10–13]) and the strain-induced metal to insulator transitions in superconductors with relaxation of ions around point defects.[14]

In our prior investigation, a combination of computational techniques (Density Functional Theory and Molecular Dynamic calculations) and experimental data provided a detailed understanding of the atomistic factors responsible for chemical expansion in fluorite structured ceria and zirconia. Chemical expansion was found to be the result of two competing processes: (1) lattice contraction around an oxygen vacancy (primarily due to electrostatic interactions) and (2) lattice expansion or contraction from the change in the cation radius (primarily due to steric effects).[15,16] Often the latter quantity is much larger (*e.g.* reduction of Ce^{4+} to Ce^{3+}, or Gd^{3+} or La^{3+} doping in CeO_2), resulting in a net expansion. To describe the contraction in the former process, the radius of a vacancy, an empirical parameter describing lattice relaxation, was introduced and shown to be smaller than that of an oxygen ion. Interestingly, the magnitude of relaxation around a vacancy was found to be larger in zirconia than in ceria, and solid solutions of the two were subsequently demonstrated as a novel method for reducing chemical expansion of ceria.[17] In order to provide a

[a]Department of Materials Science and Engineering, MIT, Cambridge, USA
[b]School of Chemistry, Trinity College Dublin, Dublin 2, Ireland
[c]Department of Nuclear Science and Engineering, MIT, Cambridge, USA. E-mail: dmarrocc@mit.edu
[d]International Institute for Carbon Neutral Energy Research (I²CNER), Kyushu University, Nishi-ku, Fukuoka, Japan
[e]Department of Materials, Imperial College London, UK

better physical understanding of the relaxation around the vacancy and thus to correlate the relaxation to structural and electrical properties, the present manuscript explores, on the atomic level, several fluorite structured oxides (ZrO_2, HfO_2, CeO_2, UO_2, and Bi_2O_3). We used a meta-analysis of available experimental data combined with new modeling data derived from state-of-the-art molecular dynamics simulations. Three key observations are discussed: the drive for monoclinic transformation for small host cations (*i.e.* Zr and Hf) is readily observed by asymmetric distortions in lattice relaxation; with increasing host cation size, an observed increase in relaxation around vacancies is related to decreasing long range repulsion of cations; examination of the strain relaxation over several unit cells demonstrated that oxygen vacancies will interact with each other over <10 Å distance. Additionally, the role of vacancy relaxation on energy of vacancy migration is discussed.

Methodology

As performed in the authors' earlier work,[16] the chemical expansion coefficient for the materials studied was extracted from the literature using lattice parameter data as a function of trivalent dopant content (either fixed valent [*e.g.* Y^{3+}] or multivalent [*e.g.* $Ce^{4+/3+}$]). In this work, the chemical expansion coefficient, α_C, of a general oxide of chemical formula $A_xB_{1-x}O_{2-x/2}$ (where B is a tetravalent cation and A a trivalent acceptor dopant), is defined *via* the following relationship:

$$\varepsilon = (a - a_0)/a_0 = \alpha_C x, \quad (1)$$

where ε is the lattice parameter expansion or chemical expansion, a and a_0 are the lattice parameters of the stoichiometric oxide, BO_2, and the nonstoichiometric one, $A_xB_{1-x}O_{2-x/2}$. The chemical expansion coefficients obtained from the literature data on different fluorite-structured oxides are reported in Table 1, along with their standard deviation. The effective radius of an oxygen vacancy, r_V, was calculated from α_C using the equations derived in our previous work:[16]

$$r_V = r_O + 4(r_h + r_O)(\alpha_C - \alpha_M) = r_O + 4(r_h + r_O)\alpha_V, \quad (2)$$

where r_O and r_h are the radius of the oxygen ion (1.38 Å) and the host cation, taken from Shannon.[18] α_M is the cation chemical expansion coefficient, defined as:

$$\alpha_M = (r_s - r_h)/(r_h + r_O), \quad (3)$$

Table 1 Vacancy chemical expansion coefficient, α_V, and vacancy radius, r_V, extracted from experimental data. The last column reports the references from which the experimental data were obtained

Host cation	r_h (Å)	α_V	r_V (Å)	Reference
Hf	0.83	−0.058	0.87 ± 0.03	32–34
Zr	0.84	−0.044	0.99 ± 0.04	16
Ce	0.97	−0.022	1.17 ± 0.06	16
U	1.00	−0.040	1.00 ± 0.07	35 and 36
Th	1.05	−0.020	1.18 ± 0.02	37 and 38
Bi	1.17	−0.050	0.87 ± 0.00	39 and 40

where r_s is the radius of the dopant cation, A. We also remind the reader of the relationship linking the chemical expansion coefficient to the cation (α_M) and vacancy (α_V) chemical expansion coefficients:

$$\alpha_C = \alpha_M + \alpha_V. \quad (4)$$

Molecular Dynamics (MD) simulations were performed to complement and interpret the experimental data. The interaction potential used for the molecular dynamics simulations of CeO_2 and ZrO_2 is known as the DIPole Polarizable Ion Model (DIPPIM) and includes a pair potential (a Buckingham-like term plus Coulombic interactions), together with an account of the polarization effects that result from the induction of dipoles on the ions.[19–22] This reads:

$$V = \sum_{i \le j} \frac{q_i q_j}{r_{ij}} + \sum_{i \le j} \frac{A^{ij} e^{a^{ij} r_{ij}}}{r_{ij}} + V_{disp} + V_{pol}\ , \quad (5)$$

where V_{disp} and V_{pol} are the dispersion and polarization terms and are described in ref. 22. The parameterization and testing of this model for CeO_2 and ZrO_2 were reported in previous publications.[15,23] The accuracy of this model was found to be similar to that of DFT calculations, and the lower computational cost allows the performance of longer simulations on bigger systems. The lattice parameters for the studied systems were obtained by performing molecular dynamics simulations with 4 × 4 × 4 supercells (~768 atoms) in an NPT ensemble, at the required temperatures. The host and dopant cations were randomly distributed. While there is experimental evidence of cation clustering in some of these materials,[24–26] these tendencies are usually linked to the size mismatch between host and dopant cation, which, in this case, is zero (see below). An isotropic barostat and thermostat were used as described by Martyna *et al.* and the external pressure was set to zero.[27,28] The isotropic barostat (NPT) was preferred to the anisotropic one (NST) because it is more robust (stable) and therefore more apt to simulate these high temperature materials. The isotropic barostat therefore enforced a cubic fluorite symmetry to the simulation box, though local, lower-symmetry relaxations around a vacancy can still be observed (see below). The lattice parameters were usually averaged over long trajectories (<0.1 ns), at high temperature (1000 K). Running these calculations at high temperature has a series of advantages. First of all, defect ordering (especially vacancy ordering[29,30]) is expected to be minimal at these temperatures, a desirable feature since ordering is known to affect the lattice parameter.[31] Second, high temperature (and the isotropic barostat) stabilize (at least partially) the fluorite structure for those compounds (such as HfO_2 and ZrO_2) that are not fluorite-structured at low temperature. All these calculations were performed with an in-house code called PIMAIM. The DIPPIM potential has also been recently implemented in the freely available CP2K code.[58]

In addition to CeO_2 and ZrO_2, we also studied other compositions in which the host cation had a different radius to that of Zr or Ce. This ranged from a value smaller than Hf (0.79 Å) to one comparable to Bi (1.17 Å). This was achieved by

Table 2 Vacancy chemical expansion coefficient, α_V, and vacancy radius, r_V, extracted from MD calculations

r_h (Å)	α_V	r_V (Å)
0.79	−0.061	0.84 ± 0.03
0.84	−0.058	0.86 ± 0.03
0.89	−0.048	0.94 ± 0.03
0.97	−0.032	1.08 ± 0.03
1.02	−0.035	1.04 ± 0.03
1.07	−0.037	1.02 ± 0.03
1.12	−0.039	0.99 ± 0.03
1.17	−0.041	0.96 ± 0.03

manually modifying the host cation–anion short-range interaction parameters of the potentials, *i.e.* both A^{ij} and a^{ij}, which are directly related to the cation size. We note here that, while this procedure yields cations with radii similar to known compounds, such as Bi_2O_3, the interaction potential is not fully representative of these compounds because other parameters, such as the polarization and dispersion coefficients, have been left unchanged. Also, we warn the reader that there is more than one combination of A^{ij} and a^{ij} that can give a certain ionic radius (and lattice parameter) and that these might predict different out-of-equilibrium properties of the material (such as elastic constants). In the present study, only equilibrium is of concern, thus the above consideration can be safely ignored. As demonstrated below, the validity of this approach is confirmed by comparison with experimental data.

The procedure to obtain the vacancy radius was as follows: first, the host cation–oxygen interaction parameters (taken from either the CeO_2 or ZrO_2 potential) were scaled in order to change the host cation radius to the desired value (0.79, 0.89, 1.02, 1.07, 1.12, 1.17 Å). This was confirmed by monitoring changes in the cation–anion bond distance obtained from the radial distribution functions.[16] Once the host cation had the desired radius, the dopant cation–anion short range parameter was scaled so that now the dopant cation radius was the same as the host cation. In the cases of CeO_2 and ZrO_2, these dopant cations are the so-called "equal-radius" Ce^{3+} and "equal-radius" Y^{3+} cations introduced in our previous work.[16] Similarly, for the other compounds in this study, the dopant cations are treated as a trivalent acceptor with a radius that is equal to the host cation. The resulting lattice parameters were used to calculate the chemical expansion (ε) of this material and, by plotting ε *vs.* dopant concentration (x), we extracted α_C (see eqn (1)). The vacancy radius was then calculated from α_C using eqn (2) and the fact that $\alpha_M = 0$ in these materials (because the dopant cation has the same radius as the host cation).[16] These data are reported in Table 2. An error of ~0.03 Å for r_V from the computational calculations is estimated from the statistical error when deriving α_C from a linear fit.

Results

Table 1 shows the experimentally derived (see eqn (2)) lattice relaxation around an oxygen vacancy for a series of fluorite structured oxides, quantified by the chemical expansion coefficient for a vacancy (α_V) and its corresponding effective radius in the lattice (r_V), with the latter plotted in Fig. 1. With increasing host cation size, the magnitude of expansion goes through a minimum, and the corresponding r_V goes through a maximum (though with a value consistently below the radius for an oxide ion = 1.38 Å, as shown by the blue dashed line), both indicating that relaxation around a vacancy is least near Ce and largest near the Hf and Bi end members. Some deviation from the indicated trend in Fig. 1 is observed for the experimental data, particularly for UO_2 and ThO_2, and most likely reflects the relatively small amount of available experimental data as compared to, for example, CeO_2, where more than ten independent measurements were averaged. In Table 2, and plotted in Fig. 1, the same data are reported as derived from simulations. The results from the MD simulations agree quite well with the experimental data, as they also show, quite clearly, a maximum in r_V for $r_h \sim 1$ Å. The agreement is not always quantitative, but this is expected considering the spread observed in the experimental data (chemical expansion coefficient can sometimes differ by more than 50%, see ref. 16) and the semi-empirical approach used to change the host cation radius in the MD simulations (which, for instance, does not take into account changes in the cation polarizability).

In addition to predicting the above macroscale properties (verified by experiment) an advantage of computational techniques is their insight into the local atomic structure, such as the relaxation pattern of ions around defects.[5,16,17] The relaxations of ions around oxygen vacancies are reported in Fig. 2, for three host cation radii (r_h = 0.79, 0.97 and 1.17 Å, denoted Small Cation [SC], Intermediate Cation [IC], and Large Cation [LC], respectively). The positions of ions close to a vacancy (black cube) are shown, with blue [green] arrows indicating anion [cation] displacements greater than 0.14 Å with respect to the perfect crystal (obtained from a structure optimization at 0 K). As expected, anions move towards the vacancy and cations are repelled (with oxide ions displaced along the (100) or equivalent

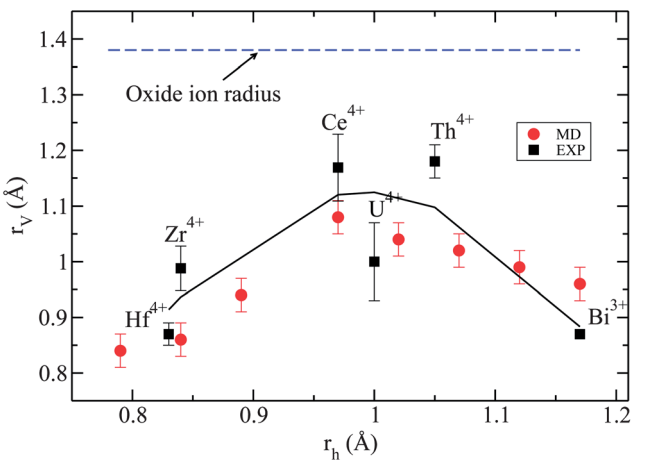

Fig. 1 Experimental (black squares) and simulated (red points) vacancy radius (a measure of lattice relaxation around a vacancy) as a function of the host cation radius. The black line is a guide to the eye and the blue dashed line is the oxide ion radius (1.38 Å).

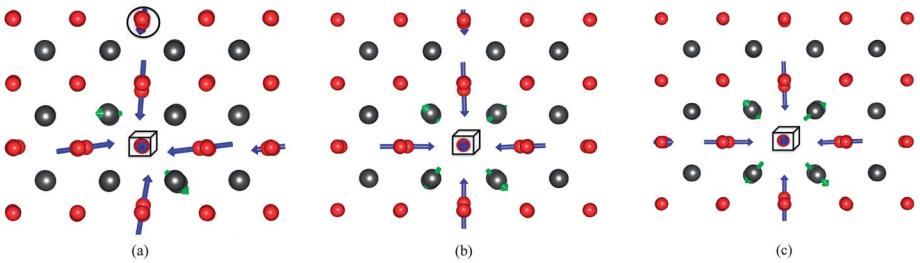

Fig. 2 Local relaxations around a vacancy (black cube) in BO_2 oxides, with $r_h = 0.79$ Å (a), 0.97 Å (b) and 1.17 Å (c). Red and grey spheres are oxygen and cerium atoms, respectively. The blue (green) thick arrows indicate the anion (cation) displacements greater than 0.14 Å, with the arrow length corresponding (for clarity's sake) to four times the displacement of the ion.

directions and cations displaced along the (111) direction for IC and LC), as discussed in the introduction.[41] Interestingly, the relaxation pattern for SC (Fig. 2a) exhibits lower symmetry than for both IC and LC, indicating that vacancies not only lead to a relaxation, but that the relaxation configuration depends on host cation size (a finding also discussed in ref. 17).

From the atomic arrangements shown in Fig. 2, the radial distribution functions ($g(r)$), a measure of the probability of finding an atom at a distance r away from a given reference atom for different ion/vacancy pairs were calculated, as shown in Fig. 3 and 4 (see ref. 21,42–45 for an explanation of how $g(r)$ is calculated and examples of their uses in solid state chemistry). In Fig. 3a and b and 4a, the $g(r)$ for oxygen ions paired with a central oxygen ion as well as the same oxygen ions paired with a central vacancy for the SC, IC, and LC, respectively, are shown. Clearly, in each case the presence of an oxygen vacancy leads to a relaxation of oxygen ions towards the vacancy, with the displacements from the ideal structure extending to at least the 4th nearest neighbor oxygen shell (corresponding to the 4th peak in the $g(r)$, indicated by the blue arrow in Fig. 3a and highlighted in Fig. 2a by a black circle). The distortions in the crystal caused by the presence of a vacancy only begin to die out at long distances, as exemplified by the overlap of the V–O and O–O $g(r)$s for distances greater than ~5 Å. Additionally, while the $g(r)$s for

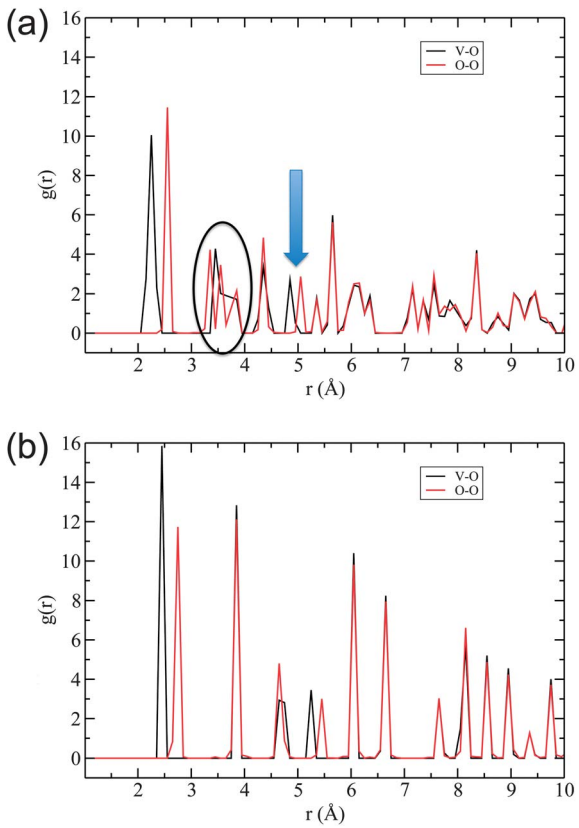

Fig. 3 Vacancy–oxygen and oxygen–oxygen radial distribution functions ($g(r)$) extracted from the ionic positions shown in Fig. 2 for SC (a) and IC (b).

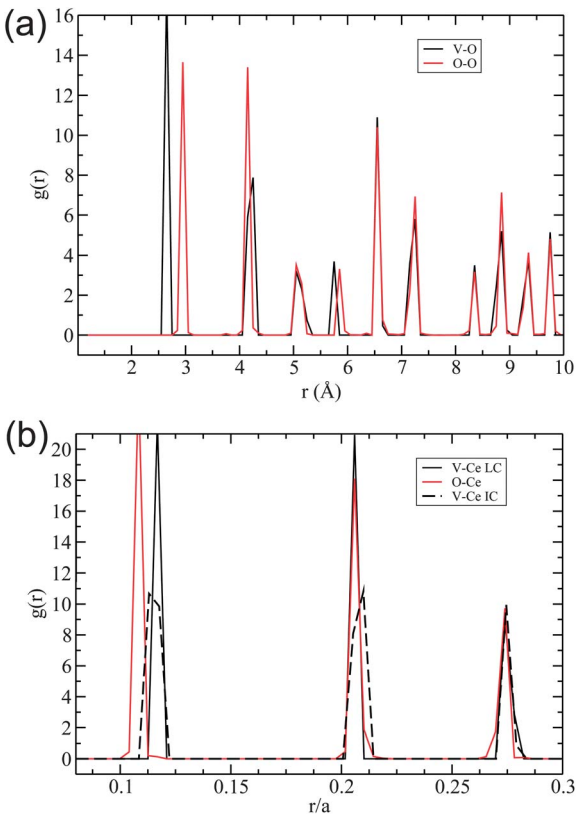

Fig. 4 Vacancy–oxygen and oxygen–oxygen radial distribution functions ($g(r)$) extracted from the ionic positions shown in Fig. 2 for LC (a). Vacancy–cation and oxygen–cation $g(r)$s are shown for IC and LC in (b). The distance, r, of the radial distribution functions was rescaled by the lattice parameters of the material (a_{IC} or a_{LC}), to facilitate the comparison.

IC and LC present sharp peaks at distances expected for the respective coordination shells in the fluorite structure, the SC material exhibits broader peaks, occasionally split into doublet or triplet sets of peaks (see black circle in Fig. 3a).

Fig. 4b shows the vacancy–cation $g(r)$s for the IC and LC materials as well as a reference anion–cation $g(r)$ for IC material. The distance, r, in the LC and IC $g(r)$s was divided by the lattice parameter of their respective materials, to allow for comparison between materials with different lattice parameters. As expected, the first peak in the vacancy–cation $g(r)$ of both materials (solid and dashed black lines) is significantly shifted to longer distance as compared to the reference anion–cation $g(r)$ (red line), confirming that the cations displace away from the vacancy as discussed in the introduction. However, turning to the second peak, the LC material exhibits little to no displacement from the reference, whereas the IC material presents a significant displacement away from the vacancy. The impact of this and the above results on understanding lattice relaxations in these materials is discussed in the next section.

Discussion

In Fig. 1, the vacancy radius clearly exhibits a maximum as a function of the host cation radius at approximately $r_h \sim 1$ Å (*i.e.* near CeO_2 and ThO_2). This behavior is analogous to the (strain driven) critical dopant radius for minimal vacancy – substitutional cation binding energy, observed in ceria and zirconia.[9,46,47] However, the relaxation patterns in Fig. 2 only exhibit an obvious change from SC to IC, with similar behavior shown in Fig. 3 for IC and LC. Substantial, asymmetric anion relaxations are observed for SC (~0.3 Å for the six nearest neighbor oxygen ions) and rather small cation relaxations – only two of the four nearest neighbor cations present displacements greater than 0.14 Å. The structure of this material appears to locally relax to a non-cubic crystalline structure, with a subsequent significant contraction around the vacancy, which leads to a very small value of the vacancy radius. Due to their size, such small host cations prefer a coordination number smaller than 8 (*e.g.* ZrO_2 and HfO_2) and it is therefore expected that the SC exhibits such asymmetric relaxation patterns. Indeed, a geometrically based rule of thumb is that the cubic fluorite structure is stable for $r_h/r_O > 0.7$, which corresponds approximately to the Ce^{4+} cation. Therefore, the distortion trends in Fig. 1–3 with cation sizes below that for Ce^{4+} are primarily associated with this cubic structure instability.

Turning now to the IC and LC materials, one finds the oxide ion displacements as shown in Fig. 3b and 4a are very similar, and seemingly counterintuitive, since, as shown in Fig. 1, the vacancy radius changes quite substantially (~0.12 Å) between the two. However, upon examination of Fig. 4b, one finds that for IC, larger cation displacements are observed as compared to those for LC, meaning that larger cations relax less and therefore, for similar anion displacements, LC exhibits a smaller vacancy radius. Two factors probably contribute to this effect. First, from a steric perspective, the larger cation radius of LC will make it harder for the second shell of cations to displace away from the vacancy. Second, the Coulombic repulsion that drives the cation displacements in the second shell will be smaller because of the greater initial distance between the vacancy and these cations in LC (again a consequence of the larger cation radius in LC). The displacements observed, in IC, for the second shell of cations around the vacancy are not very large (~0.05 Å) but there are 12 second cation nearest neighbors compared to only 4 in the nearest neighbor position, meaning that the overall effect is significant.

It is stimulating at this point to make a comparison of the trend in Fig. 1 with activation energy for ionic conduction. Considering that ionic conduction proceeds *via* oxide ion hopping through vacancies (introduced by acceptor doping), it would come as no surprise that a lower amount of relaxation (*i.e.* larger vacancy radius) should yield a lower barrier towards migration. Indeed one typically observes higher oxygen migration energies for ZrO_2 (SC material) as compared to CeO_2 (IC material) based ionic conductors.[48,49] The energy barrier to oxygen migration consists of two parts: an intrinsic contribution and an association, or trapping, term, with the latter dependent on the acceptor dopant type and concentration.[9,50] For the cubic ionic conductors ZrO_2, HfO_2, and CeO_2, the intrinsic barrier is approximately equal (E_A = 0.64–0.68 eV), reflecting little impact of the lattice parameter on the migration energy.[51–56] On the other hand, the association term varies considerably with dopant cation ($E_A \sim 0.1$ to 1 eV) and is largely attributed to a size mismatch between host† and dopant cation.[29,30,46,47,57–59] Since a larger number of acceptor dopants with radii comparable to Ce are available, as compared to Zr, often lower association energies are observed for CeO_2.[60] The role of lattice relaxation around oxygen vacancies, as studied here, on association energy has previously not been explicitly considered. One can imagine that a distortion in the lattice created by a dopant will serve to trap a vacancy when that vacancy creates a large distortion in the lattice as well. On the other hand, for a vacancy which creates minimal distortion in the lattice, on a strain basis, there is little difference between a vacancy and the oxide ion and therefore less drive to trap the vacancy. The oxygen vacancy migration is schematically shown in Fig. 5 for SC and IC cases. The intrinsic migration energy (H_i) remains constant for the two materials, but the association energy (H_a) is larger for the SC case where there is greater relaxation around a vacancy. Therefore, in CeO_2, where lattice relaxation around a vacancy is smaller as compared to ZrO_2, the impact of dopant-host size mismatch should also be smaller. Though further work is required to validate this theory, this result indicates that relaxation around vacancies plays a significant role in ionic conduction. Indeed, overcoming lattice volume relaxation around defect clusters containing vacancies has been suggested to be the primary reason for the increase in ionic conductivity of tensile strained ionic conductors.[61] Lastly, the small ion migration energy observed for the LC material, which would correspond to δ-Bi_2O_3 ($H_i \sim 0.2$ to 0.4 eV), as compared to the IC group of materials, is a result of a lone pair

† In fact, the size mismatch is between the dopant radius and a critical radius, slightly larger than the host cation size (see corresponding citations for more details).

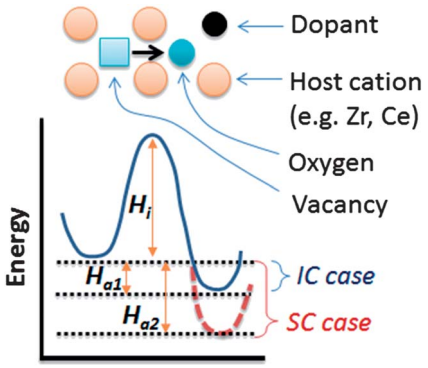

Fig. 5 Schematic of oxygen vacancy migration in an ionic crystal indicating the potential increase of association energy (H_a) with increased lattice relaxation around a vacancy in SC material as compared to IC material.

of electrons leading to highly polarizable cation in the material with a consequent disordered, "liquid-like" anion sublattice.[62–70] For ThO_2 and UO_2 there is insufficient ionic conductivity data in the literature to make similar comparisons.

The finding that lattice distortions induced by vacancies are fairly long-range, and that they die out only at distances greater than the critical value ($r^* \sim 5$ Å), merits further discussion. Indeed, there is much interest, in the solid state ionics field, in determining the conditions at which defects start interacting with each other, since this can significantly affect the conducting, structural and mechanical properties of these materials.[71–74] Fig. 3 shows that a vacancy significantly affects the positions of neighboring anions up to the fourth coordination shell. Therefore vacancies will begin to "sense", or interact with, each other at a distance smaller than twice r^*. Assuming vacancies are randomly distributed (though interactions with dopant cations may lead to a non-random distribution, particularly for high concentrations[17,23,25,26,29,30,45,75–77]), the probability of a vacancy *not* having another vacancy within a radius equal to $2r^*$ is given by

$$p(\%) = 100\prod_{i=1}^{12}(1-c)^{X_i}$$

where c is the vacancy concentration and X_i the number of i^{th} nearest neighbors.[75] In this case the product runs up to the 12^{th} neighbor shell, corresponding to a vacancy–vacancy distance of approximately 10 Å. The probability values for different vacancy concentrations are reported in Table 3. It can be seen that even for a 1% vacancy concentration there is already an ~87% probability that two vacancies will be closer than ~10 Å. Defining a critical vacancy concentration, c^*, by a two standard deviation criterion (*i.e.* a probability >95% that vacancies are non-interacting), we obtain $c^* = 0.025\%$. This concentration is more than two orders of magnitude smaller than that used to obtain necessary levels of ionic conductivity, for example, in solid oxide fuel cell materials such as ceria and zirconia. This confirms the experimental findings that defects interact very strongly in these materials.

Table 3 Probability for different vacancy concentrations that two vacancies are *not* within ~10 Å of each other, and therefore interacting by strain

c (%)	Probability (%)
0.015	97
0.025	95
0.05	90
0.1	82
0.5	36
1	13
2.5	0.57
5	0.003

Conclusions

The chemical expansion coefficient and the relaxation patterns around an oxygen vacancy, in fluorite-structured oxides, was studied as a function of the host cation radius. This was done by combining an analysis of data from the literature with new molecular dynamics simulations. A trend was observed in the effective radius of an oxygen vacancy which presents a maximum for a value of the host cation close to that of cerium ($r_h = 0.97$ Å). The observed behavior was divided into two regimes. For host cations smaller than Ce^{4+}, *i.e.* $r_h/r_O < 0.7$, the fluorite structure was found to be unstable and the relaxations around a vacancy present an asymmetric relaxation pattern, that leads to a significant contraction of the lattice (in agreement with the very small vacancy radii). When the host cation radius is equal or greater than that of Ce^{4+}, the fluorite structure is stable and the relaxation pattern around a vacancy has a cubic symmetry. In this regime, the vacancy chemical expansion coefficient, α_v, decreases as the host cation radius is increased, though rather slowly. This behavior has been ascribed to differences in the relaxation pattern of the second shell of cations. Additionally, increased lattice relaxation around vacancies is suggested to result in increasing vacancy–dopant association energy (with corresponding increases in vacancy migration energy). Finally, a careful analysis of the vacancy–anion radial distribution functions of these materials provided insight onto the spatial extension of the relaxations around a vacancy and allowed an estimate for a critical vacancy concentration, $c^* = 0.025\%$, above which vacancies start interacting.

Acknowledgements

DM wishes to thank the Government of Ireland for an EMPOWER Postdoctoral Fellowship and the Trinity Center for High Performance Computing. The SFI/HEA Irish Centre for High-End Computing (allocations tcche026b, tcche031b and tcche034b) is also thanked for the provision of computational facilities and support. Support from the NSF XSEDE program (allocation TG-DMR110004) is also acknowledged. DM is thankful to Profs. Harry Tuller and Bilge Yildiz for his recent appointment as visiting scientist at MIT and to Prof. Graeme Watson (Trinity College Dublin) for his mentorship and previous work on chemical expansion. SRB acknowledges support from WPI-I2CNER supported by the World Premier International Research Initiative (WPI), MEXT, Japan and the Basic Energy Sciences, U. S. Department of Energy (award DE-SC0002633).

References

1 S. B. Adler, *Chem. Rev.*, 2004, **104**, 4791–4843.
2 B. C. H. Steele and A. Heinzel, *Nature*, 2001, **414**, 345–352.
3 M. Sugiura, *Catal. Surv. Asia*, 2003, **7**, 77–87.
4 A. Trovarelli, *Catal. Rev.: Sci. Eng.*, 1996, **38**, 439–520.
5 H.-F. Wang, Y.-L. Guo, G.-Z. Lu and P. Hu, *Angew. Chem., Int. Ed.*, 2009, **48**, 8289–8292.
6 A. B. Kehoe, D. O. Scanlon and G. W. Watson, *Chem. Mater.*, 2011, **23**, 4464–4468.
7 W. C. Chueh, C. Falter, M. Abbott, D. Scipio, P. Furler, S. M. Haile and A. Steinfeld, *Science*, 2010, **330**, 1797–1801.
8 S. B. Adler, *J. Am. Ceram. Soc.*, 2001, **84**, 2117–2119.
9 J. A. Kilner, *Solid State Ionics*, 2000, **129**, 13–23.
10 Y. M. Chiang, *Science*, 2010, **330**, 1485–1486.
11 W. H. Woodford, Y. M. Chiang and W. C. Carter, *J. Electrochem. Soc.*, 2010, **157**, A1052–A1059.
12 M. Qu, W. H. Woodford, J. M. Maloney, W. C. Carter, Y. M. Chiang and K. J. Van Vliet, *Adv. Energy Mater.*, 2012, **2**, 940–944.
13 W. H. Woodford, W. C. Carter and Y. M. Chiang, *Energy Environ. Sci.*, 2012, **5**, 8014–8024.
14 Y. Kuru, M. Usman, G. Cristiani and H. U. Habermeier, *J. Cryst. Growth*, 2010, **312**, 2904–2908.
15 M. Burbano, D. Marrocchelli, B. Yildiz, H. L. Tuller, S. T. Norberg, S. Hull, P. A. Madden and G. W. Watson, *J. Phys.: Condens. Matter*, 2011, **23**, 255402.
16 D. Marrocchelli, S. R. Bishop, H. L. Tuller and B. Yildiz, *Adv. Funct. Mater.*, 2012, **22**, 1958.
17 S. M. Bishop, D. Marrocchelli, W. Fang, K. Amezawa, K. Yashiro and G. Watson, *Energy Environ. Sci.*, 2013, **6**, 1142–1146.
18 R. D. Shannon, *Acta Crystallogr., Sect. A: Cryst. Phys., Diffr., Theor. Gen. Crystallogr.*, 1976, **32**, 751–767.
19 B. Rotenberg, M. Salanne, C. Simon and R. Vuilleumier, *Phys. Rev. Lett.*, 2010, **104**, 138301.
20 M. Salanne and P. A. Madden, *Mol. Phys.*, 2011, **109**, 2299–2315.
21 M. Salanne, D. Marrocchelli and G. W. Watson, *J. Phys. Chem. C*, 2012, **116**, 18618.
22 M. Salanne, B. Rotenberg, S. Jahn, R. Vuilleumier, C. Simon and P. A. Madden, *Theor. Chem. Acc.*, 2012, **131**, 16.
23 S. T. Norberg, I. Ahmed, S. Hull, D. Marrocchelli and P. A. Madden, *J. Phys.: Condens. Matter*, 2009, **21**, 215401.
24 D. R. Ou, T. Mori, F. Ye, T. Kobayashi, J. Zou, G. Auchterlonie and J. Drennan, *Appl. Phys. Lett.*, 2006, **89**, 171911.
25 F. Ye, T. Mori, D. Ou, A. Cormack, R. Lewis and J. Drennan, *Solid State Ionics*, 2008, **179**, 1962–1967.
26 F. Ye, T. Mori, D. R. Ou and A. N. Cormack, *Solid State Ionics*, 2009, **180**, 1127–1132.
27 G. J. Martyna, *Phys. Rev. E: Stat. Phys., Plasmas, Fluids, Relat. Interdiscip. Top.*, 1994, **50**, 3234–3236.
28 G. J. Martyna, D. J. Tobias and M. L. Klein, *J. Chem. Phys.*, 1994, **101**, 4177–4189.
29 D. Marrocchelli, P. A. Madden, S. T. Norberg and S. Hull, *Chem. Mater.*, 2011, **23**, 1365–1373.
30 S. T. Norberg, S. Hull, I. Ahmed, S. G. Eriksson, D. Marrocchelli, P. A. Madden, P. Li and J. T. S. Irvine, *Chem. Mater.*, 2011, **23**, 1356–1364.
31 S. Bishop, K. Duncan and E. Wachsman, *Electrochim. Acta*, 2009, **54**, 1436–1443.
32 C. Pascual and P. Duran, *J. Mater. Sci.*, 1982, **17**, 3431–3436.
33 P. Duran and C. Pascual, *J. Mater. Sci.*, 1984, **19**, 1178–1184.
34 D. J. Kim, S. H. Hyun, S. G. Kim and M. Yashima, *J. Am. Ceram. Soc.*, 1994, **77**, 597–599.
35 L. Desgranges, Y. Pontillon, P. Matheron, M. Marcet, P. Simon, G. Guimbretiere and F. Porcher, *Inorg. Chem.*, 2012, **51**, 9147–9149.
36 T. L. Markin and R. S. Street, *J. Inorg. Nucl. Chem.*, 1967, **29**, 2265–2280.
37 M. Aizenshtein, T. Y. Shvareva and A. Navrotsky, *J. Am. Ceram. Soc.*, 2010, **93**, 4142–4147.
38 M. D. Mathews, B. R. Ambekar and A. K. Tyagi, *J. Alloys Compd.*, 2005, **386**, 234–237.
39 T. Takahashi, H. Iwahara and T. Esaka, *J. Electrochem. Soc.*, 1977, **124**, 1563–1569.
40 R. S. Roth and J. L. Waring, *J. Res. Natl. Bur. Stand., Sect. A*, 1962, **66**, 451–463.
41 We note here that these calculations differ from the ones reported in our previous work. Indeed, the present results are obtained from a structure relaxation on a $4 \times 4 \times 4$ unit cell simulation box, in which the dopant cation has been purposely placed far away from the vacancy ($\sim$10 A). Our previous calculations, based on Density Functional Theory, were on a smaller $2 \times 2 \times 2$ unit cell box and the dopant cations (Ce^{3+}) were nearest neighbours of the vacancy. This explains why the magnitude of the ionic displacements differs slightly.
42 M. Coduri, M. Brunelli, M. Scavini, M. Allieta, P. Masala, L. Capogna, H. E. Fischer and C. Ferrero, *Zeitschrift Fur Kristallographie*, 2012, **227**, 272–279.
43 M. Scavini, M. Coduri, M. Allieta, M. Brune and C. Ferrero, *Chem. Mater.*, 2012, **24**, 1338–1345.
44 D. Chandler, *Introduction to Modern Statistical Mechanics*, Oxford University Press, 1987.
45 S. Hull, S. T. Norberg, I. Ahmed, S. G. Eriksson, D. Marrocchelli and P. A. Madden, *J. Solid State Chem.*, 2009, **182**, 2815–2821.
46 L. Minervini, M. O. Zacate and R. W. Grimes, *Solid State Ionics*, 1999, **116**, 339–349.
47 M. O. Zacate, L. Minervini, D. J. Bradfield, R. W. Grimes and K. E. Sickafus, *Solid State Ionics*, 2000, **128**, 243–254.
48 P. S. Manning, J. D. Sirman, R. A. DeSouza and J. A. Kilner, *Solid State Ionics*, 1997, **100**, 1–10.
49 J. Faber, C. Geoffroy, A. Roux, A. Sylvestre and P. Abelard, *Appl. Phys. A: Mater. Sci. Process.*, 1989, **49**, 225–232.
50 J. A. Kilner and R. J. Brook, *Solid State Ionics*, 1982, **6**, 237–252.
51 J. E. Bauerle and J. Hrizo, *J. Phys. Chem. Solids*, 1969, **30**, 565.
52 T. Politova, *Solid State Ionics*, 2004, **168**, 153–165.
53 D. Y. Wang, D. S. Park, J. Griffith and A. S. Nowick, *Solid State Ionics*, 1981, **2**, 95–105.
54 S. Omar, E. D. Wachsman and J. C. Nino, *Solid State Ionics*, 2008, **178**, 1890–1897.

55 B. C. H. Steele, *Solid State Ionics*, 2000, **129**, 95–110.
56 M. F. Trubelja and V. S. Stubican, *Solid State Ionics*, 1991, **49**, 89–97.
57 D. A. Andersson, S. I. Simak, N. V. Skorodumova, I. A. Abrikosov and B. Johansson, *Proc. Natl. Acad. Sci. U. S. A.*, 2006, **103**, 3518–3521.
58 M. Nakayama and M. Martin, *Phys. Chem. Chem. Phys.*, 2009, **11**, 3241–3249.
59 M. Burbano, S. T. Norberg, S. Hull, S. G. Eriksson, D. Marrocchelli, P. A. Madden and G. W. Watson, *Chem. Mater.*, 2012, **24**, 222–229.
60 B. C. H. Steele, *Solid State Ionics*, 1984, **12**, 391–406.
61 M. J. D. Rushton, A. Chroneos, S. J. Skinner, J. A. Kilner and R. W. Grimes, *Solid State Ionics*, 2013, **230**, 37–42.
62 N. X. Jiang, E. D. Wachsman and S. H. Jung, *Solid State Ionics*, 2002, **150**, 347–353.
63 P. Shuk, H. D. Wiemhofer, U. Guth, W. Gopel and M. Greenblatt, *Solid State Ionics*, 1996, **89**, 179–196.
64 S. Hull, S. T. Norberg, M. G. Tucker, S. G. Eriksson, C. E. Mohn and S. Stolen, *Dalton Trans.*, 2009, 8737–8745.
65 C. E. Mohn, S. Stolen, S. T. Norberg and S. Hull, *Phys. Rev. B: Condens. Matter Mater. Phys.*, 2009, **80**, 024205.
66 C. E. Mohn, S. Stolen, S. T. Norberg and S. Hull, *Phys. Rev. Lett.*, 2009, **102**, 155502.
67 I. Abrahams, X. Liu, S. Hull, S. T. Norberg, F. Krok, A. Kozanecka-Szmigiel, M. S. Islam and S. J. Stokes, *Chem. Mater.*, 2010, **22**, 4435–4445.
68 X. Liu, I. Abrahams, S. Hull, S. T. Norberg, M. Holdynski and F. Krok, *Solid State Ionics*, 2011, **192**, 176–180.
69 S. T. Norberg, S. G. Eriksson and S. Hull, *Solid State Ionics*, 2011, **192**, 409–412.
70 P. D. Battle, C. R. A. Catlow, J. W. Heap and L. M. Moroney, *J. Solid State Chem.*, 1986, **63**, 8–15.
71 A. Kossoy, Y. Feldman, R. Korobko, E. Wachtel, I. Lubomirsky and J. Maier, *Adv. Funct. Mater.*, 2009, **19**, 634–641.
72 A. Kossoy, Y. Feldman, E. Wachtel, I. Lubomirsky and J. Maier, *Adv. Funct. Mater.*, 2007, **17**, 2393–2398.
73 A. Kossoy, A. I. Frenkel, Q. Wang, E. Wachtel and I. Lubomirsky, *Adv. Mater.*, 2010, **22**, 1659–1662.
74 H. L. Tuller and S. R. Bishop, *Annu. Rev. Mater. Res.*, 2011, **41**, 369–398.
75 B. Wang and A. N. Cormack, *J. Phys. Chem. C*, 2012, **117**, 146–151.
76 J. P. Goff, W. Hayes, S. Hull, M. T. Hutchings and K. N. Clausen, *Phys. Rev. B: Condens. Matter Mater. Phys.*, 1999, **59**, 14202–14219.
77 D. Marrocchelli, P. A. Madden, S. T. Norberg and S. Hull, *J. Phys.: Condens. Matter*, 2009, **21**, 405403.

